

# ECLIPSE INSTRUMENT TO RECORD THE POLARIZATION OF THE FLASH SPECTRUM

ALEX FELLER, JAN O. STENFLO \* and DANIEL GISLER  
*Institute of Astronomy, ETH Zurich, 8092 Zurich, Switzerland*

and

RENZO RAMELLI  
*Istituto Ricerche Solari Locarno, Via Patocchi, CH-6605, Locarno, Switzerland*

**Abstract.** We have designed and built an instrument to capture the polarization of the flash spectrum during a total solar eclipse. The whole visible spectral range, from UV to the near IR, is covered with a spectral resolution of 3000. The sampling period is about 20 ms, which corresponds to a height resolution of some 10 km in the solar atmosphere. The instrument is composed of an 8-inch Dall-Kirkham type telescope and a slitless spectropolarimeter. The F/11.5 telescope beam projects a solar image in its focal plane, where the entrance aperture of the spectropolarimeter cuts a 2.5 arcmin slice of the solar limb. The resulting beam is split into two orthogonally polarized components by means of a Savart plate. Before entering the spectrograph the beam is reduced to F/2.8 to have sufficient illumination on the detector. The measurements are only feasible during an eclipse, since seeing and stray light prohibit a clean isolation of the chromospheric light with a coronagraph. The flash spectrum has been successfully recorded during the eclipse of March 29, 2006.

**Key words:** polarization, solar eclipse, flash spectrum

## 1. Introduction

The chromospheric emission spectrum, called flash spectrum, has already been recorded successfully during multiple eclipse expeditions (Cillié and Menzel, 1935; Mitchell, 1947; Dunn *et al.*, 1968; Shen *et al.*, 1981). The mentioned authors have compiled catalogues itemizing the calibrated absolute fluxes of more than a thousand emission lines in the range 300 to 910 nm. The spectra of Dunn *et al.* (1968) cover 4500 km on the Sun with a height resolution of 100 km in the direction of lunar movement. Although these data lack polarization information, they have been very helpful for the design of our instrument, allowing us to narrow down the required sensitivity range.

In terms of polarimetry we know of two past eclipse observations. The measurements in the Ca II H and K lines of Hanson *et al.* (1976) allowed a 5% upper limit to be set on the K line degree of polarization. Moreover, from his visual tracking of the intensity variations produced by a rotating polaroid screen, Stokley (1948) estimated that the overall degree of polarization of the flash spectrum is probably not above 10%. This result is however questionable because of the rapid exponential drop of the line intensities during the flash phase.

---

\* also affiliated with the Faculty of Mathematics & Science, University of Zurich

The flash spectrum is extremely difficult to observe outside an eclipse. The steep intensity decrease at the extreme limb of the Sun makes a coronagraph very vulnerable to stray light caused by the earth's atmosphere and by the optics of the instrument itself. The main challenge here is the occulting disc. It must not exceed the solar disc by more than a fraction of an arcsecond, to properly isolate the thin chromospheric layer from the photosphere while still leaving it uncovered. Another serious drawback of out-of-eclipse observations is the spatial resolution of current solar telescopes, which is limited to about 100 km. In contrast, as the eclipsing Moon is moving at a relative speed of about 350 km/s, a height resolution of order 10 km on the Sun can already be achieved with a moderate frame rate of 50 frames/s.

When using the Moon as occulting disc one has to take into account that the lunar limb is somewhat serrated. For the 29 March 2006 eclipse, the lunar limb profile at the positions of second and third contact (Espenak and Anderson, 2004) shows typical height variations corresponding to about 700 km on the Sun. On the other hand, the lunar mountains and valleys can be easily resolved with a modest spatial resolution of about 5'' in the direction parallel to the Moon's limb, which allows for a later correction of the chromospheric height scale across the field of view.

The scientific rationale of our observations is described in detail by Stenflo (2006). A theoretical reference has been developed by Chandrasekhar (1950) in terms of an idealized model for a plane-parallel purely scattering atmosphere. The conditions at the extreme limb of the Sun are approaching this Chandrasekhar limit, but the real polarization can nevertheless be significantly influenced by different physical processes: the relative importance of different opacities, collisions, deviation from plane-parallel stratification (spherical geometry at the limb, small scale inhomogeneities), atomic physics (quantum interference, optical pumping), radiative-transfer physics and magnetic fields (Hanle effect). These processes affect the individual spectral lines in different ways. By recording a large part of the spectrum, we may be able to untangle and quantify them with the help of differential diagnostics.

## 2. Instrument design

TABLE I  
Main instrument characteristics.

spectral range	340 - 870 nm
spectral sampling	0.21 nm/pixel
time resolution	13 - 40 ms
spatial sampling	5''/pixel
field of view	150''

### 2.1. PHOTON BUDGET

When designing a polarimeter one has to make a trade-off between spatial, spectral, and time resolution and polarimetric sensitivity (Table I). The chromospheric sickle is not resolved in practice in the direction of lunar movement, because of the steep

POLARIZATION OF THE FLASH SPECTRUM

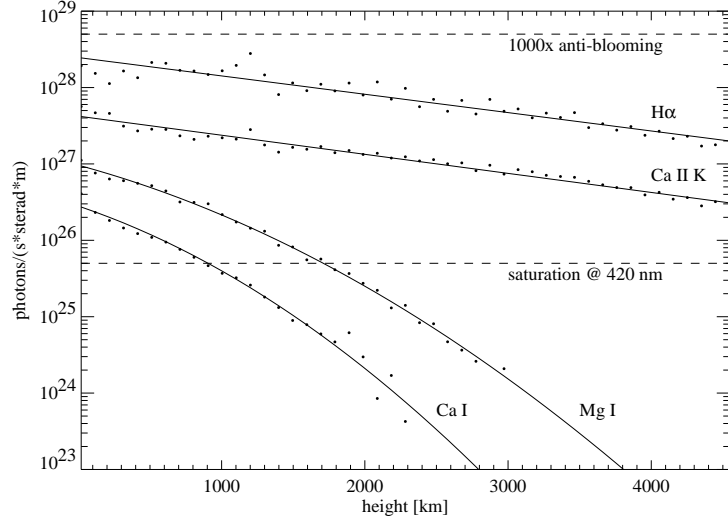


Fig. 1. Flux variation with height for some selected emission lines of Table II. Data are from Dunn *et al.* (1968). For our purpose, the logarithm of the flux can be sufficiently well fitted with a linear function for the strong lines and a second order polynomial for the weak lines. The estimated saturation level around Ca I and the corresponding anti-blooming limit are indicated by the dashed lines.

TABLE II  
Lines of interest sorted by flux

Line	Wavelength nm	flux at $h=0^\dagger$ $\text{photons} \cdot \text{s}^{-1} \cdot \text{sterad}^{-1} \cdot \text{m}^{-1}$
H $\alpha$	656.3	$2.0 \cdot 10^{28}$
Ca II	854.2	$9.4 \cdot 10^{27}$
Ca II	866.2	$8.7 \cdot 10^{27}$
Ca II K	393.3	$5.5 \cdot 10^{27}$
H $\beta$	486.1	$5.4 \cdot 10^{27}$
Ca II H	396.8	$4.8 \cdot 10^{27}$
Ca II	849.8	$4.3 \cdot 10^{27}$
He D <sub>3</sub>	587.6	$3.5 \cdot 10^{27}$
Mg I	518.4	$1.3 \cdot 10^{27}$
Na I D <sub>2</sub>	589.0	$8.9 \cdot 10^{26}$
Na I D <sub>1</sub>	589.6	$8.9 \cdot 10^{26}$
Mg I	516.7	$7.8 \cdot 10^{26}$
Mg I	517.2	$7.8 \cdot 10^{26}$
Ca I	422.7	$4.3 \cdot 10^{26}$

$^\dagger$  from Dunn *et al.* (1968)

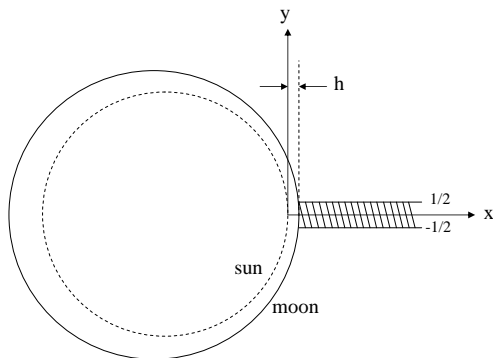


Fig. 2. Definition of the integrated flux from a chromospheric emission line.

intensity drop with height (see Fig. 1). The spectral line profile is not resolved either. In this context it is convenient to define, for a given line  $i$ , an integrated flux  $F_i$  given by

$$F_i(h) = \int_h^\infty \int_{-1/2}^{1/2} \int_{\lambda_i - \Delta\lambda_i/2}^{\lambda_i + \Delta\lambda_i/2} f(\lambda) d\lambda dy dx \quad (1)$$

Thus  $F_i(h)$  is the total number of photons per second and sterad, emitted from a one unit thick semi-infinite slab of the chromosphere at height  $h$  (see Fig. 2) and within a spectral window  $\Delta\lambda_i$  around the line center  $\lambda_i$ .

Given the flux  $F_i$ , we can then determine the total number of photoelectrons generated in a camera pixel.

$$N_i(h) = F_i(h) \Delta\Omega \Delta y \Delta t \epsilon_{\text{opt}} q_{\text{eff}}(\lambda_i) \quad (2)$$

$\Delta\Omega$  is the solid angle covered by the instrument aperture, as seen from the Sun,  $\Delta y$  is the extent along the chromospheric sickle imaged by the pixel, and  $\Delta t$  is the exposure time.  $\epsilon_{\text{opt}}$  refers to the total transmission of the atmosphere and the optics and  $q_{\text{eff}}$  to the quantum efficiency of the camera. As the product of atmospheric extinction and quantum efficiency is changing by a factor of 5 across the spectral working range, its wavelength dependence must be taken into account. The optics are roughly estimated to contribute to the total efficiency with a factor of 0.1.

The huge dynamic range between  $H\alpha$  and the weak lines (see Fig. 1 and Table II) cannot be handled by the camera at once. At maximum frame rate the instrument has to be sensitive enough to just saturate in the Ca I line at the beginning of the flash phase. The stronger lines will then drop into the sensitivity range later on. Unfortunately the  $H\alpha$  flux indicated by Dunn (1968) for  $h = 0$  is not consistent with the flux at the center of the  $H\alpha$  absorption line at the photospheric limb, which is an order of magnitude lower. This uncertainty is however not critical for the optical design as an instrument that is too fast can easily be dimmed. In addition the flux in the weak lines is decreasing steeply enough to stop saturating the camera after the first few seconds into the flash phase. On the other hand it is important to

TABLE III  
Camera characteristics

CCD size	4096 pixels × 96 pixels
pixel size	13 μm × 13 μm
dark current at 30 °C	1.23 · 10 <sup>3</sup> e <sup>-</sup> /s
readout noise	70 e <sup>-</sup>
sampling	50 e <sup>-</sup> /count, 10 bit
readout time	6 ms/frame
frame rate <sup>†</sup>	1.53 - 75 frames/s
anti-blooming factor	1000

<sup>†</sup> limited by the mechanical shutter

have a CCD with an anti-blooming feature of at least 1000 × saturation, to avoid any crosstalk from the strong lines during the saturated phase. As we were able to obtain a very fast F/2.8 spectrograph, we can adequately expose the camera with a modest and easily transportable 8-inch telescope (see Fig. 3).

The noise in the measured degree of polarization  $Q/I$  is, in case of a beam splitting polarimeter,

$$\sigma \approx \sqrt{\frac{1}{N} + \frac{N_{\text{dc}}}{N^2} + \frac{\sigma_{\text{readout}}^2}{N^2}} \quad , \quad (3)$$

where  $N$  is the number of photoelectrons,  $N_{\text{dc}}$  the number of electrons generated by the dark current and  $\sigma_{\text{readout}}$  the readout noise. All noise sources are assumed to be Poisson distributed. Close to saturation,  $\sigma$  is dominated by the shot noise  $N^{-1/2} \approx 0.004$ . This meets the requirements on polarimetric precision and is adequately sampled with a 10 bit A/D conversion (*cf.* Table III). At less than 0.1 × saturation the readout noise begins to dominate.  $N_{\text{dc}}$  stays below 0.001 × saturation and its contribution to the polarimetric noise is negligible.

## 2.2. TELESCOPE AND SPECTROPOLARIMETER UNIT

The telescope is an 8-inch Dall-Kirkham Cassegrain reflector. The imaging is nearly diffraction limited within our small field of view and the Cassegrain design is virtually free of instrumental polarization.

A scaled drawing and a close-up photograph of the spectropolarimeter unit are shown in Fig. 3. To keep the optical efficiency high and chromatic aberrations at a minimum, the use of glass in the beam path is avoided, except for the half wave plate and the beam splitter. At the telescope focus one can choose between a 50 μm slit of length 1.6 mm and an aperture of 1.6 mm × 1.6 mm. With the slit we record calibration spectra of the solar disk or a spectral lamp. The aperture is used for the actual observation of the flash spectrum. This slitless mode has some important advantages: it allows the imaging of extended solar structures and relaxes the tolerances on guiding and pointing of the telescope. Then again we observed disadvantages like aberrations caused by an off-axis position of the sickle or the smearing of nearby spectral lines.

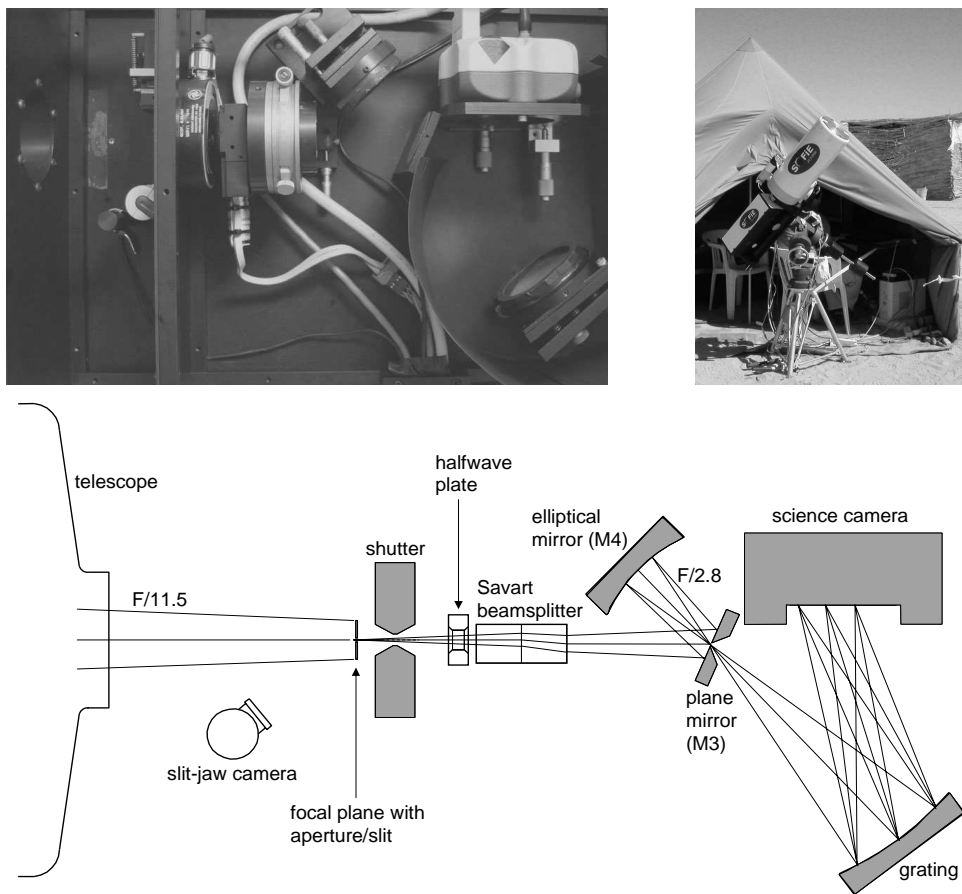


Fig. 3. **Bottom:** optical setup. **Top left:** top view of the spectropolarimeter unit. **Top right:** overview of the setup at the eclipse site near Waw an Namos, Libya. The spectropolarimeter unit is mounted behind the telescope. In the background one can see the tent which is used as work place and protection for the electronic equipment. The electrical power of the whole setup (150-200 W) is provided by fuel generators and secured with a UPS.

In terms of polarimetry we opt for a beam splitter, as opposed to the more accurate modulation/demodulation principle normally used in our Zurich Imaging Polarimeter (Povel, 1995; Gandorfer *et al.*, 2004). The arguments in favor of a beam splitter are the intricacies involved in developing an adequate achromatic modulator, and the low frame rate of our ZIMPOL cameras ( $\sim 1$  frame/s). Therefore a Savart beam splitter is used. It is installed in the slower F/11.5 beam to keep its aberrations below the size of a pixel. The disadvantage of this position is the need of rather thick calcite elements. We have  $2 \times 22.8$  mm, giving us a beam separation between 3.40 and 3.76 mm, depending on wavelength. To eliminate the effect of the polarization dependent grating efficiency, the beam splitter has to be turned so that the polarization direction of both beams is oriented  $\pm 45^\circ$  to the grooves of the grating. A half wave plate is needed in this context to realign the Moon's limb with the

direction of Stokes  $+Q$ . We renounce the use of true beam exchange again because of the intricacies of getting an adequate fast-switchable and achromatic half wave plate. Instead the retarder is turned mechanically by  $45^\circ$  one single time between the two flash phases of second and third contact.

After the Savart plate the two beams are deflected by a plane mirror (M3) with a circular hole of 2.5 mm diameter, reduced by an elliptical mirror (M4) to F/2.8 and then focused through the hole in M3 into the spectrograph. This configuration allows to use M4 on-axis, and the hole only causes a small loss of about 5% of the flux. The focal points of M4 slightly deviate from their paraxial positions (telescope focus and intermediary focus at M3) to minimize the differential aberrations between cospatial image points in the two beams.

The spectrograph consists of an aberration corrected holographic concave grating with 405 grooves/mm, serving as both the dispersive and focussing element. Operated in first order it provides a practically linear dispersion of 0.21 nm/pixel over the whole wavelength range. The efficiency varies between about 45% (393 nm) and 23% (866 nm). We find however a significant residual astigmatism, clearly dominating the total aberrations of the instrument. As a trade-off we adjust the grating and camera position to align the detector plane as good as possible with the spectral focal plane, but accepting therefore a strong wavelength dependent spatial defocussing.

Both the telescope and the spectropolarimeter unit are assembled on a paralactic mounting with computer-controlled stepping motors on both axes (*cf.* Sect. 2.3). The guiding and pointing accuracies in the hour axis are limited by the worm gear which has a period of about 12 minutes at guiding speed and a mean amplitude of some  $40''$ . Due to their periodicity, the hour axis errors can at least be partly compensated with the guiding software. The guiding and pointing accuracies in the declination axis are of order  $1''$ /minute and  $10''$  respectively and can be neglected for our purpose. The knowledge of the pointing accuracies is crucial for the eclipse observations as the telescope has to be moved blindly to the opposite limb during totality (*cf.* Sect. 2.3). It defines the minimum size of the aperture in the spectropolarimeter unit.

### 2.3. INSTRUMENT CONTROL AND OBSERVING PROCEDURE

Figure 4 shows a block diagram of the different control units and programs. The control tasks are allocated to three different computers: Computer I is responsible for the guiding and acts as time server, computer II is used for monitoring the solar disc, and computer III is handling the spectropolarimeter unit.

The telescope mounting is aligned by star tracking according to the Bigourdan procedure. For accurate pointing on the Sun a special guiding software has been developed in-house which uses the solar limb as reference frame. The pointing position is determined by scanning the solar disc in the two axis directions with the spectropolarimeter in slit-mode, and determining the limb position by the corresponding inflection point in the measured intensity.

The time server is providing UTC with an accuracy of about 10 ms, which corresponds to the time resolution of the instrument.

The science camera and shutter as well as the rotation of the half wave plate

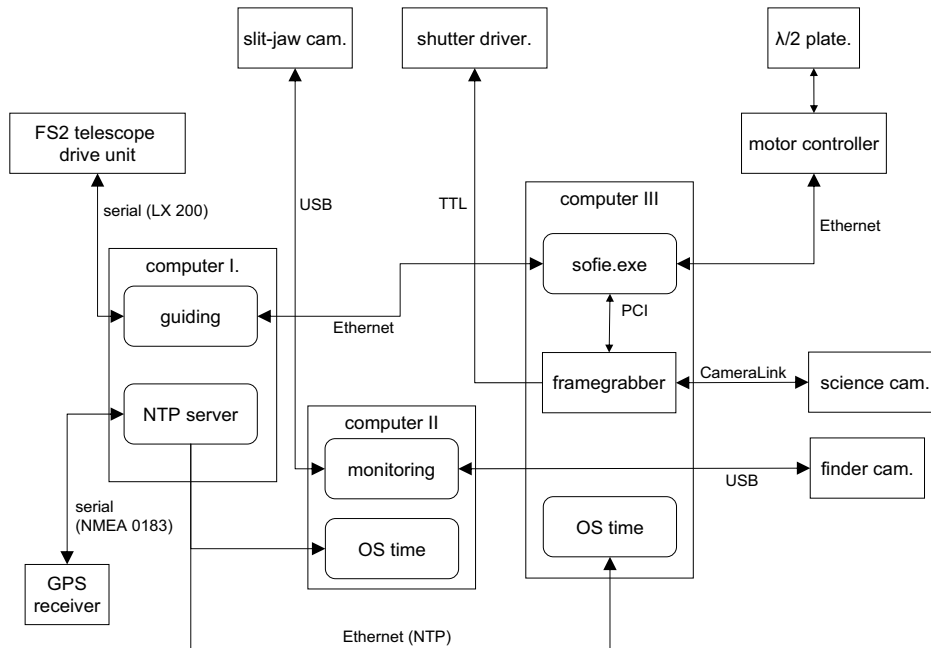


Fig. 4. Control units and programs for the eclipse instrument. The boxes with the soft edges denote computer programs, the boxes with sharp edges hardware devices. The lines of communication are annotated with the connection type and/or the protocol.

are controlled with software developed in-house and optimized for the particular requirements of the eclipse observation. A critical item is the reliable handling of the data stream, which is reaching 56 MB/s at maximum frame rate. Other important features are the live display of the science camera images and the possibility to quickly adjust the frame rate during operation.

TABLE IV  
Location

Latitude	24:28:03 N
Longitude	17:57:52 E
Altitude	450 m

Table V summarizes all the relevant observing and calibration procedures together with the respective timings. Our observing spot is located near Waw an Namos in the Sahara of southern Libya (*cf.* Table IV), on the center line of the eclipse path and close to the point of maximum duration of totality. The center-line position is necessary to avoid sickle movements during the flash phases, while the long duration of totality is of advantage for extending the duration of the flash

TABLE V  
Observing procedure

UTC	Events
	Limb scan to set the guiding reference frame Position the slit at the predicted position of first contact (angle $135.2^\circ$ )
08:55:54.67	First contact Verify the positioning accuracy and the orientation of the spectropolarimeter unit
	Move to the predicted position of second contact (angle $-44.7^\circ$ ) Limb scan including the lunar limb to correct the guiding reference frame Change from slit to aperture
10:13:30	Open the telescope Start recording with a fixed rate of 25 frames/s
10:13:45.20	Second contact
10:14:34	Slow down to 1.5 frames/s for the coronal lines Move to predicted position of third contact (angle $136.9^\circ$ ) Rotate half wave plate by $45^\circ$ for beam exchange
10:17:14	Start with variable frame rate program: the frame rates are incremented from 25 to 75 frames/s in steps of 25 frames/s, based upon a visual rating of the flash intensity
10:17:55.74	Third contact
10:18:16	Close telescope Stop recording Change back to slit Polarimetric calibration at disc center Dark current/bias and flat field measurements Spectral calibration with Rb I lamp

phases.

### 3. Conclusions and outlook

The instrument described here has been developed and built from scratch within one year for the 29 March 2006 eclipse. The observing location in the desert, hundreds of km away from any infrastructure, called for robust, compact, reliable and completely autonomous equipment as well as elaborate logistics.

Despite all these challenges the equipment was running faultlessly. The eclipse was passing under ideal weather conditions and we were able to measure both flash phases of second and third contacts, on opposite solar limb positions (*cf.* Table V).

Our requirements were however not entirely satisfied. The main drawback of the instrument is the residual aberrations caused by the grating, in particular the differential effects between the two beams (*cf.* Fig. 5). They have been discovered only during the tests of the final instrument, and we were not able to fully resolve them in due time. On the other hand the slitless mode has proven to be an advantage for isolated spectral lines like  $H\alpha$ , allowing to image extended structures like a prominence, but a disadvantage for adjacent lines like He  $D_3$ , Na  $D_1$  and  $D_2$ .

Frame= 460, UT= 10:13:46.466

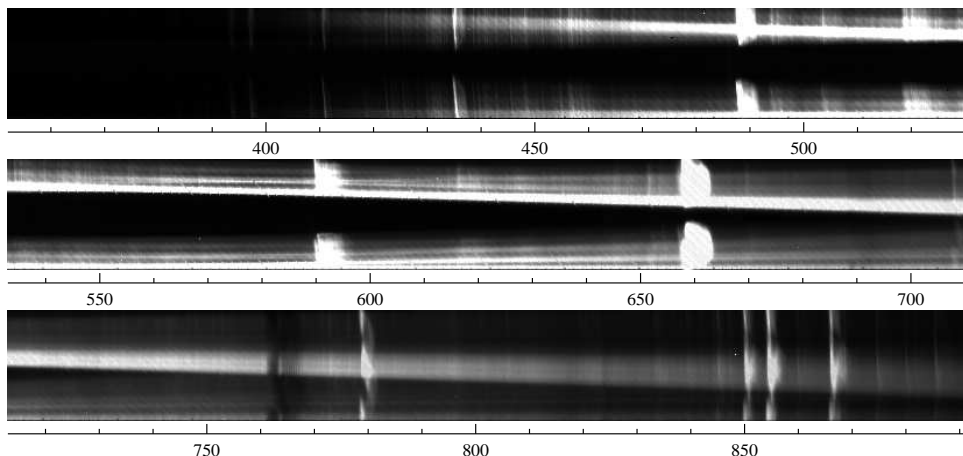


Fig. 5. Sample frame from the flash phase at second contact, representing the raw data (only corrected for bias and flat field). The scale gives the wavelength in nm. The two orthogonally polarized spectra are imaged above each other. Since the separation between them is strongly wavelength dependent, they are well separated in the UV (so well that vignetting is severe), while they significantly overlap in the infrared. While some strong lines, like  $H\beta$ , the Helium D3 lines, and  $H\alpha$ , are still saturated in this particular frame, the Ca H and K lines in the UV are already quite faint. The almost horizontal bright band represents the remaining part of the photospheric sickle. In this frame one can discern the main instrumental problems: vignetting, overlap, and aberrations, in particular the differential effects between the two spectra.

The data reduction is still ongoing, and the results as well as the reduction techniques will be discussed in detail in a later publication. The main challenge is to study and model the aberrations in order to determine the cospatial regions in both images and to improve the spatial resolution in some parts of the spectrum.

Finally we are already thinking of incorporating our experiences for a second generation eclipse experiment. The key enhancements we will be working on are the replacement of the slitless mode with an array of optical fibers, the use of an Echelle grating, and a true achromatic beam exchange.

**Acknowledgements.** Financial support for this work has been obtained through grants Nos. 200020-101603 and 200020-109159 from Swiss Nationalfonds. We would like to thank the technical staff at the Institute of Astronomy of ETH Zurich as well as Michele Bianda and Evio Tognini from the Istituto Ricerche Solari Locarno for helping with the development of the instrument and the control software and for handling the time pressure so calmly. We are also grateful to the Specola Solare Ticinese in Locarno, for having made available to us a very convenient testing environment, and to Osama Shalabiea and the Sebha University for their kind support in Libya.

## References

- Chandrasekhar, S.: 1950, *Radiative Transfer*, Clarendon Press, Oxford  
 Cillié, G.G. and Menzel, D.H.: 1935, *Harvard College Obs. Circ.*, **410**, 1  
 del Toro Iniesta, J.C. and Collados, M.: 2000, *Appl. Opt.* **39**, 1637  
 Dunn, R.B., Evans, J.W., Jefferies, J.T., Orrall, F.Q., White, O.R., and Zirker, J.B.: 1968, *ApJS*,

POLARIZATION OF THE FLASH SPECTRUM

**15**, 275

- Espenak, F. and Anderson, J.: 2004, *NASA Technical Paper No. 212762*  
Gandorfer, A. M. et al.: 2004, *A&A*, **422**, 703  
Hanson, T., Stenholm, B., Söderhjelm, S.: 1976, *Reports from the Observatory of Lund, No. 8*  
Mitchell, S.A.: 1947, *ApJ*, **105**, 1  
Povel, H.P.: 1995, *Opt. Eng.*, **34**, 1870  
Shen L., Li, Q., Yu, J., Sun, R.: 1981, *Chin. A&A*, **5**, 388  
Stenflo, J.O.: 2006, these proceedings  
Stokley, J.: 1948, *AJ*, **53**, 117